PHYSICAL REVIEW E **72**, 030102(R) (2005)

Intrinsic coherence resonance in an electrochemical cell

M. Rivera,[1] Gerardo J. Escalera Santos,[2] J. Uruchurtu-Chavarín,[3] and P. Parmananda[1,2]
[1]*Centro de Ciencias Físicas, UNAM, Cuernavaca 62210, Morelos, México*
[2]*Facultad de Ciencias, UAEM, Avenida Universidad 1001, Colonia Chamilpa, Cuernavaca, Morelos, México*
[3]*CIICAP, UAEM, Avenida Universidad 1001, Colonia Chamilpa, Cuernavaca, Morelos, México*
(Received 26 January 2005; revised manuscript received 15 June 2005; published 16 September 2005)

We study the interaction of intrinsic electrochemical noise with autonomous nonlinear dynamics of a three-electrode electrochemical cell. The amplitude of this intrinsic (internal) noise, regulated by the concentration of chloride ions, is monotonically increased and the provoked dynamics is analyzed. The experimentally constructed coherence factor β versus the concentration of the chloride ions' curve has a unimodal shape indicating the emergence of intrinsic coherence resonance. The abscissa for the maxima of this unimodal curve corresponds to the optimum value of intrinsic noise where maximum regularity of the invoked dynamics is observed.

DOI: 10.1103/PhysRevE.72.030102 PACS number(s): 05.40.−a, 05.45.Xt

Stochastic resonance (SR) [1–3], the phenomena wherein the addition of external noise enhances the detection of weak subthreshold signals in nonlinear systems, has attracted a lot of attention lately. This apparently counterintuitive role of noise has been studied exhaustively both theoretically and experimentally in diverse physical, chemical, and biological systems [4–9]. A comprehensive review by Gammaitoni *et al.* [10] highlights all the important advances in this field along with the prominent references. Another important aspect of the constructive role of external noise in nonlinear systems is coherence resonance (CR) [11,12] where, even in the absence of a subthreshold deterministic signal, enhanced regularity of the provoked dynamics is observed for optimum levels of superimposed external noise. In comparison, the role of internal noise and its interaction with nonlinear dynamics [13–15] is less understood. Since it is possible to envisage numerous real systems with intrinsic noise, the question that internal noise could, similarly to its external counterpart, play a constructive role in nonlinear systems has tremendous validity and applicability. For example, it has been categorically (experimentally) shown that synaptic noise improves the detection of subthreshold signals in Hippocampal CA1 neurons [15]. Moreover, it has been shown numerically by Schmid *et al.* [14], using the Hodgkin-Huxley model [16], that internal noise caused by the fluctuations of individual channels in an assembly of ion channels can induce intrinsic coherence resonance (ICR). Consequently, for optimum levels of internal noise, the regularity of the observed spike sequence is augmented [14].

In this paper, we report the experimental observation of ICR in a three-electrode electrochemical cell. The amount of internal noise is regulated by the concentration of chloride ions in the electrolytic solution. For appropriate values of the system parameters, these chloride ions attack the anode surface stochastically through a process known in electrochemistry literature as pitting corrosion [17,18]. Increasing the concentration of chloride ions augments this stochastic activity (increased levels of internal noise), resulting in enhanced levels of pitting corrosion. It is observed that the internal-noise-provoked system dynamics exhibits ICR as a function of the concentration of chloride ions present in the electrolytic solution. This inception of ICR, evident from the regularity of the invoked time series of anodic current (I) at certain optimum levels of internal noise, is furthermore verified quantitatively by calculating the coherence factor β [19,20] defined as

$$\beta = h(\Delta\omega/\omega_p)^{-1}, \tag{1}$$

where h is the height of the dominant peak (at frequency ω_p) in the power spectra and $\Delta\omega$ is the width of this dominant peak at a height of $\exp^{-1/2} h$. It needs to be pointed out that the local fluctuations in the original power spectra were suppressed using a running average of 30 data points. This smoothed power spectra was used to determine the quantities required to calculate β. Scanning electron microscope (SEM) imaging of the anode is carried out to visualize the surface morphology of the anode surface undergoing pitting corrosion. This was, in part, done in an effort to correlate the regularity observed in the time series with the spatial organization of the pitting centers on the anodic surface.

The experimental system was comprised of a three-electrode electrochemical cell configured for studying the potentiostatic (EG&G PARC model 362 potentiostat) electrodissolution of iron in a solution of potassium sulfate and sulfuric acid. The working electrode (anode) was an iron disk (Sigma Aldrich; purity 99.8%) with 6.3 mm diam shrouded in epoxy such that the polished cross-section surface was exposed to the electrolytic solution. This restricts the corrosion process to take place solely at the surface of the anode. The electrolyte solution was a mixture of 1.0 M sulfuric acid and 0.6 M potassium sulfate for one set of experiments, whereas a mixture of 1.0 M sulfuric acid and 0.4 M potassium sulfate was used for another set of experiments. A volume of 500 ml was maintained in the electrochemical cell. The anodic potential V, measured relative to a saturated calomel electrode (SCE), was used as the control parameter. The cathode was a graphite rod, 5.0 mm diam and 2 cm long, immersed in the electrolytic solution. The following protocol was implemented as a precursor to each experimental run:

(a) The anode surface was polished with sandpaper of 600 grating and rinsed thoroughly with distilled water before being mounted in the electrochemical cell.

(b) Nitrogen gas was pumped into the cell for about 15 min to cleanse the electrochemical cell of oxygen gas.

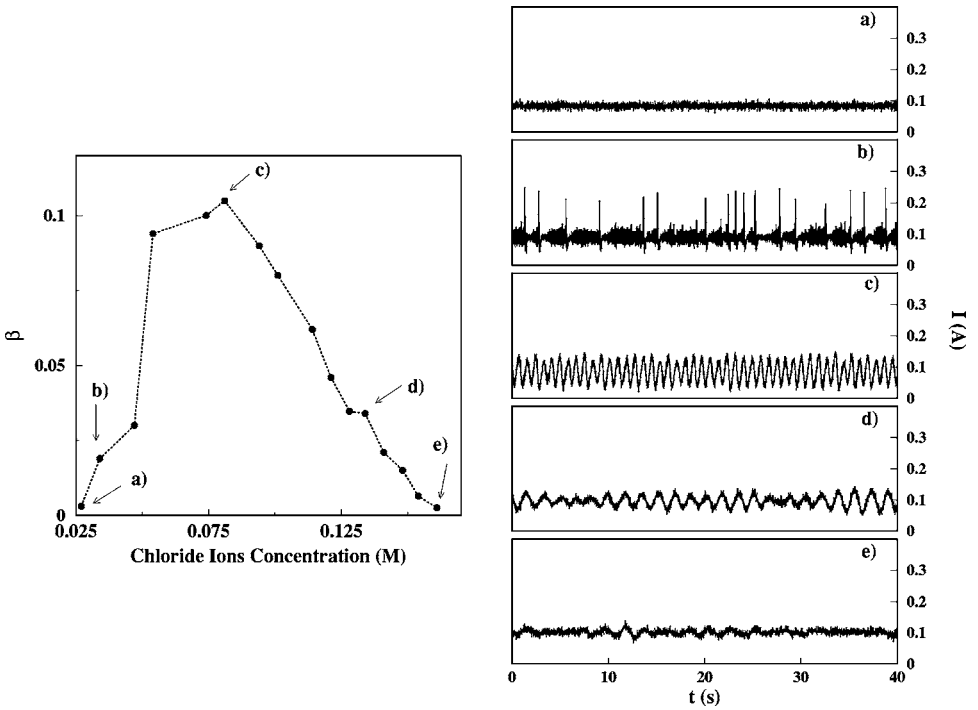

FIG. 1. The internal-noise-provoked dynamics in the electrochemical cell. The setpoint for the autonomous system is chosen to be $V_0=700$ mV and the composition of the autonomous electrolyte solution is a mixture of 1.0 M sulfuric acid and 0.6 M potassium sulfate. The left panel shows the experimentally generated coherence factor β vs concentration of chloride ions' curve. It has a unimodal shape confirming the emergence of intrinsic coherence resonance in the noise-provoked dynamics. The right panels show a section of the noise-invoked time series for the anodic current I corresponding to the experimental data points. Panels (a) and (e) show a time series corresponding to low and high levels of noise and consequently are devoid of any periodic features. Panel (c) shows a time series corresponding to an optimum level of noise and therefore is extremely regular.

Subsequently, a fixed amount of potassium chloride, our source of chloride ions (internal noise), was added to the electrolytic solution without changing the volume maintained in the electrochemical cell. After a waiting time of about 15 min, wherein the transient behavior was observed and therefore neglected, the anodic current I data (the current between the anode and the cathode) was recorded for analysis using a 12-bit data acquisition card at a sampling frequency of 200 Hz. This entire procedure is repeated for different (increasing) concentrations of chloride ions added to the electrolytic solution, analogous to monotonically increasing the amplitude of the internal noise, and the experimental β curve is constructed.

As a prelude to the experiments on ICR, the autonomous system dynamics of the electrochemical cell, in the absence of added potassium chloride, was explored using the standard cyclic voltammogram technique [21]. Different dynamical responses of the anodic current I were observed as a function of the anodic voltage V, the scan parameter [22,23]. Two basic types of dynamics were observed: steady-state fixed-point behavior with a constant current response and period-1 oscillations emerging from a supercritical Hopf bifurcation, where $V_H \approx 140$ mV. At anodic voltages slightly above the Hopf bifurcation, small, sinusoidal oscillations were observed. At higher voltages, relaxation oscillations were observed in which the period increased with an increase in voltage. This increase in period as a function of the bifurcation parameter is characteristic of a homoclinic bifurcation, such as a saddle-node or a saddle-loop bifurcation [24]. This period lengthening occurs until oscillations cease at the homoclinic bifurcation point V_{hc} at about 250 mV. It needs to be mentioned that while this cyclic voltammogram technique is not as precise as a bifurcation diagram, it is a fast and a fairly reliable method to identify the different dynamical responses observed in the distinct regions of parameter space.

Although the qualitative features of the experimental voltammogram are preserved from one experimental run to another, the exact values for the different bifurcation points may shift a little. This is, in part, due to the inevitable errors involved in the preparation of the electrolyte solution and the electrodes. In our experiments on ICR, the set point for the autonomous system was chosen to be 700 mV such that a constant anodic current I (fixed point) of about 0 mA was observed. This setpoint, maintained constant for all experimental runs, was chosen far away from the bifurcation point in an effort to minimize the effects of small variations in the autonomous dynamics. At these experimental conditions, the anode is susceptible to pitting corrosion in the presence of chloride ions, our source of internal noise. Thereafter, potassium chloride is added to the electrolytic solution in order to analyze the effect of noise on the autonomous fixed-point dynamics. It is observed that up until a certain concentration (0.025 M) of added potassium chloride, the value of the anodic current I increases, reaching a value of about 100 mA. However, the anodic current time series continues exhibiting fixed-point behavior. This concentration of potassium chlo-

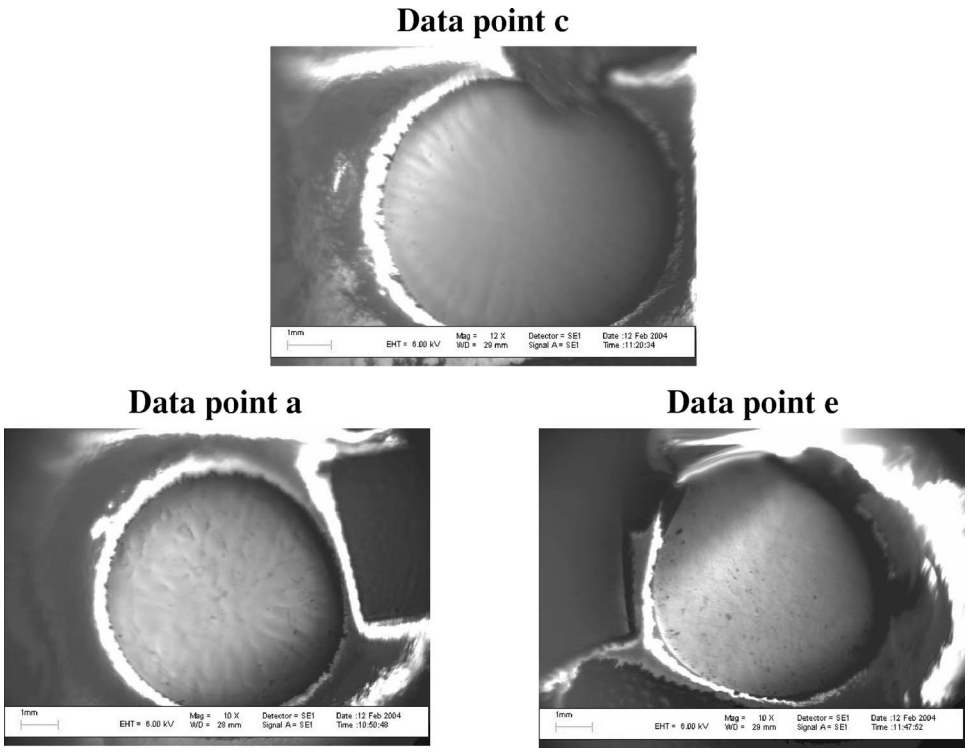

FIG. 2. SEM images revealing the morphology of the anode surface at the conclusion of three experimental runs. The images presented are a 12-fold magnification of the actual eletrode. The images are for the data points (a), (c), and (e) (extremas) of the experimentally constructed β curve shown in Fig. 1. The corresponding time series are shown in panels (a), (c), and (e) of Fig. 1.

ride, where the anodic current I exhibits fixed-point behavior at about 100 mA, is chosen to be the first point of the experimental β curve presented later. For subsequent experimental runs, each one started with fresh electrolyte solution and polished electrodes, the concentration of the added chloride ions was systematically increased, and the asymptotic time series of the anodic current (recorded for each experimental run) was used to calculate the coherence factor β. Furthermore, the surface morphology of the anode, subsequent to some experimental runs, was analyzed using the surface electron microscope.

Figure 1 shows the experimentally generated coherence factor (β) versus concentration of the chloride ions (internal-noise amplitude) curve. The time series corresponding to some of the experimental data points are shown in the adjacent panels. The computed β curve has a unimodal shape indicating the observance of ICR. It implies that for some optimum levels of internal noise the interplay of the stochastic pitting process, provoked by the chloride ions, and autonomous nonlinear dynamics invokes enhanced coherence. This is manifested by the emergence of increased regularity for oscillations presented in the time-series panel (c). In contrast, at low levels of chloride concentrations, the noise-provoked dynamics is devoid of any periodic features and for the most part exhibits fixed-point direct-current response at about 100 mA. Furthermore, at high levels of chloride concentrations, the dynamics is totally dominated by the stochastic pitting process resulting in the observance of a noisy fixed-point behavior. The profile of the provoked time series in different panels varies as different parameter domains are visited for distinct noise strengths. It is interesting to observe that the average value of the fixed-point current value for both low and high levels of internal noise remains nearly the same (100 mA).

We also tried to correlate the enhanced periodicity of the time series to the spatial organization of the anode morphology undergoing pitting corrosion. For these purposes, after some experimental runs, the anode was dismounted from the electrochemical cell and taken over to the SEM laboratory for imaging purposes. Figure 2 shows the images of the anode surface obtained, using the SEM, corresponding to points (a), (c), and (e) of the β curve shown in Fig. 1. It is observed that the anode surface corresponding to data point (c) of the β curve, where maximum coherence in the noise-induced time series is observed, exhibits increased homogeneity (smoothness) in the surface morphology. This could be due to a more regular spatial distribution of the pitting centers at this optimum level of internal noise. In contrast, the images corresponding to low (a) and high (e) levels of internal noise exhibit a substantially rougher morphology for the anode surface. It needs to be clarified that although it is interesting to detect qualitatively that SEM images indicate enhanced levels of spatial organization for optimum levels of noise, it is by no means conclusive proof for the emergence of ICR. It is the experimentally generated β curve that provides a quantitative and therefore more reliable proof for the existence of ICR in our experiments.

Figure 3 shows another experimentally generated β curve for a different composition of the autonomous electrolytic solution, that is, 1.0 M sulfuric acid and 0.4 M potassium sulfate. The autonomous dynamics for this electrolyte mixture is slightly different from the one observed in earlier experiments. Procedures identical to the ones used in previous experiments were implemented for the autonomous as well as the noise-provoked dynamics. The Fig. 3 curve, similar to its Fig. 1 counterpart, shows a unimodal shape. The time series and SEM images of the anode surface (not shown) are consistent and indicate the emergence of ICR in

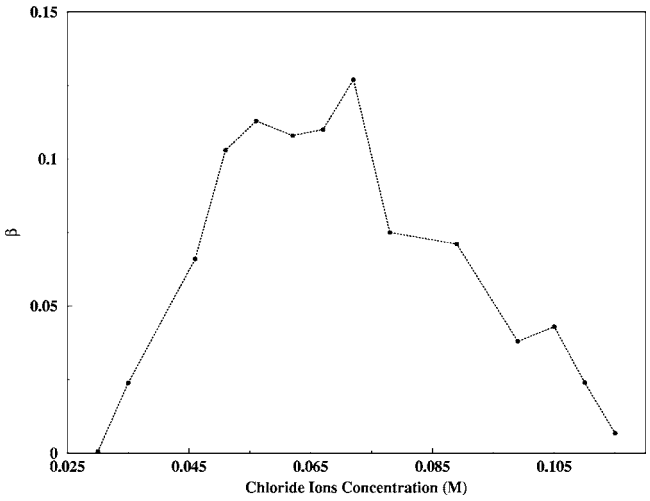

FIG. 3. The experimentally generated coherence factor β vs concentration of chloride ions' curve has a unimodal shape confirming the emergence of intrinsic coherence resonance in the noise-provoked dynamics. The setpoint for the autonomous system is chosen to be V_0=700 mV and the composition of the autonomous electrolyte solution is a mixture of 1.0 M sulfuric acid and 0.4 M potassium sulfate.

these experiments. The results of Figs. 1 and 3 furnish experimental evidence for the existence of intrinsic coherence resonance in an electrochemical cell. To reiterate, this was confirmed quantitatively by calculating the coherence factor β versus amplitude of the internal-noise curves. SEM imaging of the anode surface also indicates (qualitatively) the emergence of ICR for the noise-provoked behavior.

There have been published reports [25–28] wherein the authors used the concentration of chloride ion as a bifurcation parameter. They conclude that the chloride ions cause a localized breakdown of the passive oxide film leading to the inception of pitting corrosion and consequently complex current dynamics. Subsequently, they use a point defect model (PDF) [29], involving Schottky-pair equilibrium, to understand the physiochemical process and/or mechanism of the observed pitting corrosion. In comparison, we start with the premise that the observed pitting corrosion is a stochastic process and proceed to interpret our results within the framework of noise-induced resonances. Therefore, in our experiments, analogous to results of SR and CR for external noise, the bifurcation parameter gets varied dynamically due to the added internal noise. Furthermore, augmenting the amplitude of internal noise enables the noise-assisted dynamics to visit different domains of the bifurcation diagram. Finally, we provide both quantitative (calculation of β) and qualitative (SEM photographs of the anode surface) evidence for the emergence of ICR.

In the past there have been numerous reports involving the applications of external-noise-induced resonances such as maintenance of traveling waves, detection of subthreshold signals, enhanced sensitivity in human and/or animal response, etc. [10]. However, these applications were invariably restricted to situations where external noise can be superimposed onto the autonomous system dynamics. On the other hand, since most of the real systems in nature possess internal noise, our observation of intrinsic coherence resonance renders the noise (external and/or internal)-induced resonance phenomena ubiquitous. Furthermore, our results are of immense relevance to biological systems in general and neuronal systems in particular. For example, internal noise provoked by the fluctuation of individual channels in an assembly of ion channels induces neuronal firing [14]. In the framework of our results this would imply that as the amplitude of the internal noise is varied, different profiles of spike sequences (and consequently different interspike intervals) are generated, yielding the most regular firing pattern at an optimum value of internal noise. This would autoenable the neurophysiological sensory system to generate the desired spike train by manipulating its levels of internal noise. The omnipresence of noise-induced resonances and their possible applications to diverse nonlinear processes validate the relevance and/or importance of our experiments. Future numerical and theoretical work could enrich these experimental findings.

[1] R. Benzi *et al.*, J. Phys. A **14**, L453 (1981).
[2] R. Benzi *et al.*, Tellus **34**, 10 (1982).
[3] C. Nicolis and G. Nicolis, Tellus **33**, 225 (1981); C. Nicolis, *ibid.* **34**, 1 (1982).
[4] A. Föster *et al.*, J. Phys. Chem. **100**, 4442 (1996).
[5] T. Amemiya *et al.*, J. Phys. Chem. **102**, 4537 (1998).
[6] A. Longtin *et al.*, Phys. Rev. Lett. **67**, 656 (1991).
[7] B. Lindner *et al.*, Neural Comput. **15**, 1761 (2003).
[8] B. Lindner *et al.*, Phys. Rev. E **66**, 031916 (2002).
[9] J. J. Collins *et al.*, J. Neurophysiol. **76**, 642 (1996)
[10] L. Gammaitoni *et al.*, Rev. Mod. Phys. **70**, 223 (1998).
[11] A. S. Pikovsky and J. Kurths, Phys. Rev. Lett. **78**, 775 (1997).
[12] I. Z. Kiss *et al.*, Phys. Rev. E **67**, 035201(R) (2003).
[13] P. Jung and J. W. Shuai, Europhys. Lett. **56**, 29 (2001).
[14] G. Schmid *et al.*, Europhys. Lett. **56**, 22 (2001)
[15] William C. Stacey and Dominique M. Durand, J. Neurophysiol. **86**, 1104 (2001)
[16] A. L. Hodgkin and A. F. Huxley, J. Physiol. (London) **117**, 500 (1952).
[17] U. Bertocci, Corrosion (Houston) **35**, 211 (1979).
[18] S. B. Lalvani and G. Zhang, Corros. Sci. **37**, 1571 (1995).
[19] Hu Gang *et al.*, Phys. Rev. Lett. **71**, 807 (1993).
[20] T. Ditzinger *et al.*, Phys. Rev. E **50**, 3508 (1994).
[21] J. Wojtowicz, *Modern Aspects of Electrochemistry* (Plenum, New York, 1972), Vol. 8.
[22] A. Karantonis *et al.*, Phys. Rev. E **65**, 046213 (2002).
[23] A. Karantonis and S. Nakabayash, Chem. Phys. Lett. **347**, 133 (2001).
[24] G. J. Escalera Santos *et al.*, Phys. Rev. E **70**, 021103 (2004).
[25] Michael Pagistas *et al.*, Electrochim. Acta, **47**, 4163 (2002).
[26] Dmitra Sazou *et al.*, Electrochim. Acta **45**, 2753 (2000).
[27] Dmitra Sazou *et al.*, Chaos, Solitons Fractals, **17**, 263 (2003).
[28] Dmitra Sazou and Michael Pagistas, Chaos, Solitons Fractals, **17**, 505 (2003).
[29] D. D. Macdonald, J. Electrochem. Soc. **139**, 3434 (1992).